7th IWCIA, Int. Workshop on Combinatorial Image Analysis, R. Malgouyres (Ed.), pp. 39-56, Caen, July 2000.

Optimizing 3D chamfer masks with norm constraints

Eric Remy and Edouard Thiel

Laboratoire d'Informatique de Marseille
LIM, Case 901, 163 av Luminy, 13288 Marseille cedex 9, FRANCE
{Eric.Remy, Edouard.Thiel}@lim.univ-mrs.fr

Abstract

Chamfer distances are widely used in image analysis. One of their major interest is to approximate the Euclidean distance with integers. Optimizing approximations, in the 3D case, is done in the litterature but without worrying if the computed masks actually induce a norm. In that paper, we propose a construction of chamfer masks in 3D, based on Farey triangulations, which gives constraints on the weightings; by scanning the whole space of solutions, we compute for each mask, an exhaustive list of optimal weightings.

Keywords: Chamfer distances, discrete geometry, Farey triangulations.

1 Introduction

In image analysis, more precisely in representation and shape description, discrete geometry notions such as discrete distances are needed to measure and describe objects contained in an image. Chamfer distances, also known as weighted distances, are discrete distances which are widely used for instance when computing reversible skeletons [San94, Att97], to perform shape splitting, when interpolating two objects, when computing the generalized Voronoï diagram or when filling holes in surfaces [Akt96].

A discrete distance is positive defined, symmetric and respects the triangular inequality, and works with integers. The goal is to approximate the Euclidean distance d_E with integers, in a very efficient way both in term of storage and processing time on a whole image.

If a discrete distance satisfies the homogeneity property on the grid, then it induces a discrete norm. In most cases, it is not desirable to use a function that is a distance but not a norm, since this leads to many unpredictable results in applications, such as in medial axis extraction.

Chamfer distance can be defined in the following way: a *chamfer mask* is a set of legal displacements in a neigbourhood, each displacement being weighted by an integer cost; the *chamfer distance* between two points is the cost of the path of least cost joining them, formed with legal displacements in the mask. The notion of lattice is underlying.

Borgefors popularizes chamfer distances in [Bor84], in any dimension. Afterwards many optimization methods have been proposed, to approximate the Euclidean distance d_E; the major contribution is due to Verwer in 2 and 3 dimensions [Ver91b]. One can find in [Thi94] a complete history of chamfer distances, the comparison of different optimization methods and crossing formulas between them.

Chamfer distances have many advantages, which justify their success in applications. They are local distances, that is to say, which permit to deduce a distance from the distances of close neighbours, unlike d_E. The computation of the medial axis is also done by a local test [Thi94]. All computations are done using integer numbers and linear operations $\{+, -, <\}$.

The major attraction is the high speed — and simplicity — of the distance transform algorithm, due to Rosenfeld [Ros66]. The distance transform, denoted DT, consists in labeling each object point of an image to its distance to the complementary. The transform is global, and the Rosenfeld's algorithm operates in 2 passes on the image, independently of the thickness of the objects in the image, and of the dimension. The reverse algorithm allows to recover an object from its medial axis, also in 2 passes.

Verwer shows in [Ver91a] that any chamfer mask induces a distance. On the other hand, a chamfer mask does not necessarily induce a norm; some conditions must be fulfilled, on the choice of displacements on one side, and on the choice of associated weights on the other side.

In 2 dimensions, we have established exact conditions for a chamfer mask to induce a norm in [Thi94]. For this sake, we have established arithmetic and geometric properties of chamfer balls, and brought out general structures such as cones and elementary displacements. These results lie on Farey series, relating to the theory of numbers [Har78].

We study in this paper the chamfer balls in 3 dimensions, which structures are more complex. Indeed, switching from 2^{nd} to 3^{rd} dimension forces the loss of angular order between visible points, and the triangulation is no more unique. The construction of 3D chamfer masks we propose, is lying on Farey sets and Farey triangulations [Gra92].

In §2 we define the work space, the mask, the distance and the chamfer ball; visible points are introduced in §3 and properties of Farey sets in §4. In §5 we study the ball's geometry, the elementary displacements in the influence cones, and we introduce the notion of equivalent rational ball. The exact constraints for a chamfer mask to induce a norm are established in §6 by a convexity criterion on the ball. Hence in §7, we compute the constraints on 3 masks and we discuss in §8 the optimizations on these masks for 2 approximation criteria of d_E.

2 Definitions

Our work space is the cubic grid, associated with the fundamental lattice Λ of $\mathbb{Z}^3$. The cubic grid implies the symmetry towards planes of axes and bissectrices, called *48-symmetry*: it divides $\mathbb{Z}^3$ into 48 sub-spaces ($48 = 2^3.3!$ with 2^3 sign combinations and 3! coordinates permutations), versus 8 octants in $\mathbb{Z}^2$. We denote $\mathbb{S}$ the 48^{th} of space

$$\mathbb{S} = \left\{ 0 \leq z \leq y \leq x \,,\ (x, y, z) \in \mathbb{Z}^3 \right\} \tag{1}$$

and we denote $\mathbb{S}_n = \{(x, y, z) \in \mathbb{S},\ x \leq n\}$. In the following, we will mostly represent $\mathbb{S}$ using the projection π (figure 1) :

$$\pi : (x, y, z) \longmapsto \left(\frac{y}{x}, \frac{z}{x}\right) . \tag{2}$$

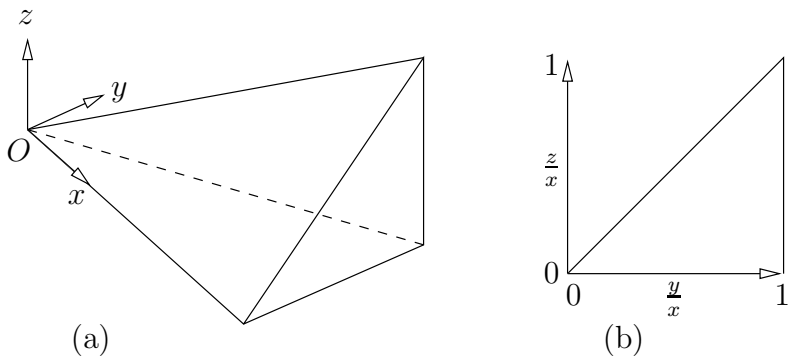

Figure 1: The 48^{th} of space $\mathbb{S}$ (a) and its representation using projection π (b).

By definition of $\mathbb{S}$, the borders of the triangle seen by projection in figure 1.b are the 3 planes passing through O such that $z = y$, $z = 0$ and $y = x$, and the triangle's interior is such that $0 < z < y < x$ (figure 2.a). We take the symmetries σ with respect to the planes delimiting $\mathbb{S}$, as illustrated figure 2.b:

$$\begin{array}{lcl} \sigma_1 : (x, y, z) & \longmapsto & (x, z, y) \\ \sigma_2 : (x, y, z) & \longmapsto & (x, y, -z) \\ \sigma_3 : (x, y, z) & \longmapsto & (y, x, z) \end{array} \qquad \begin{array}{l} \sigma_4 = \sigma_2 \circ \sigma_1 \\ \sigma_5 = \sigma_3 \circ \sigma_1 \\ \sigma_6 = \sigma_1 \circ \sigma_2 \\ \sigma_7 = \sigma_1 \circ \sigma_3 \end{array} \tag{3}$$

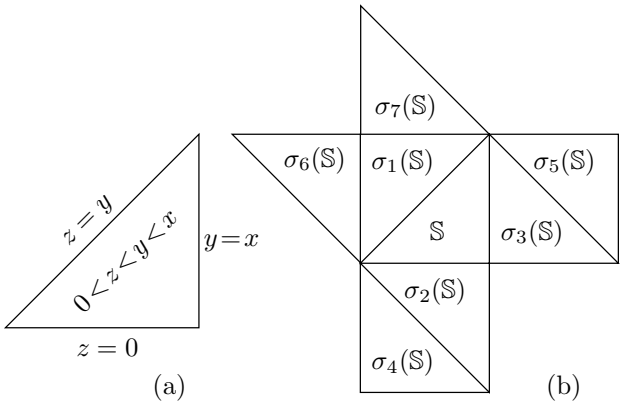

Figure 2: Planes delimiting $\mathbb{S}$ (a) and associated symmetries (b) by projection.

Definition 1 (Discrete distance) *An application $d : \mathbb{E} \times \mathbb{E} \to \mathbb{N}$ is a discrete distance on $\mathbb{E}$ iff* $\forall\ p,\ q,\ r \in \mathbb{E}$

1. $d(p, q) \geq 0$ *positive*
2. $d(p, q) = 0 \Leftrightarrow p = q$ *defined*

3. $d(p,q) = d(q,p)$ *symmetric*

4. $d(p,q) \leq d(p,r) + d(r,q)$ *triangular inequality*

Definition 2 (Discrete norm) *Let d be a discrete distance on $\mathbb{E}$. The function $n(p) = d(O,p)$ is a discrete norm iff* $\forall p \in \mathbb{E}$

5. $n(\lambda p) = |\lambda|\, n(p) \quad \forall \lambda \in \mathbb{Z}$ *homogeneous*

Definition 3 (Weighting) *We name weighting $M(x,y,z,w)$ a point $(x,y,z) \in \mathbb{Z}^3$ associated with a weight $w \in \mathbb{N}$.*

A *chamfer mask* $\mathcal{M}$ consists in a neighbourhood centered in O, of size $(2N+1)^3$, in which some displacements are authorized and weighted. In other words, $\mathcal{M}$ is a 48-symmetric set of m weightings

$$\mathcal{M} = \{\, M_i(x_i, y_i, z_i, w_i)\,,\ 1 \leq i \leq m \,\} \tag{4}$$

on which we will add some constraints. We call *generator* $\mathcal{M}^g$ of a mask $\mathcal{M}$ the part $\mathcal{M} \cap \mathbb{S}$, from which are deduced all other weightings by the 48-symmetry.

Having a mask $\mathcal{M}$, a *path* $\mathcal{P}$ is a sequence of displacements

$$\mathcal{P} = n_1 M_1 + \ldots + n_m M_m\,, \quad n_i \geq 0\ ; \tag{5}$$

the associated *cost* $W(\mathcal{P})$ of this path is

$$W(\mathcal{P}) = \sum_{i=1}^{m} n_i w_i\ . \tag{6}$$

Definition 4 (Chamfer distance) *The chamfer distance $d_{\mathcal{M}}$ between 2 points A and B is the minimum of the associated costs to all the paths $\mathcal{P}_{AB}$ from A to B:*

$$d_{\mathcal{M}}(A,B) = \min_{\mathcal{P}_{AB}}\ W(\mathcal{P}_{AB})\ . \tag{7}$$

In the following, we aim at establishing the strict norm conditions from the geometry of the chamfer ball $B_{\mathcal{M}}$ of radius $R \in \mathbb{N}$ defined as

$$B_{\mathcal{M}}(R) = \left\{\, p \in \mathbb{Z}^3 : d_{\mathcal{M}}(O,p) \leq R \,\right\} \tag{8}$$

where R is an arithmetical radius, different from the radius in number of voxel. We will see later that $B_{\mathcal{M}}$ is a discrete polyhedron.

3 Visible points

Definition 5 (Visible points) *A point $P(x,y,z) \in \mathbb{Z}^3$ is said visible (i.e visible from the origin) if no other point of the fundamental lattice is located on (OP) between O and P. A necessary and sufficient condition is* $\gcd(x,y,z) = 1$ [Har78].

The gcd of 3 integers can be expressed with the gcd of 2 integers by

$$\gcd(x, y, z) = \gcd(x, \gcd(y, z)) \tag{9}$$

in a commutative way; we recall that by definition $\gcd(x, 0) = x$; finally we remark that if x, y, z are prime and distincts, we have

$$\gcd(xy, yz, zx) = 1 \tag{10}$$

by (9) without any gcd of two of these terms beeing equal to 1.

We denote $\mathcal{V}_n$ the set of visible points of $\mathbb{S}_n$

$$\mathcal{V}_n = \{\, (x, y, z) \in \mathbb{S}_n : \gcd(x, y, z) = 1 \,\} \tag{11}$$

and we call *layer* n the subset $\mathcal{V}_n \setminus \mathcal{V}_{n-1}$.

$\mathcal{V}_n$ can be obtained with a sieve upon the periods of visible points, by scanning $\mathbb{S}_n$ on x, y, z. Visible points are numbered v_0, v_1, v_2, ... using the lexicographic order of their coordinates x, y, z ; the points of $\mathcal{V}_4$ are named a, b, c, ..., v in the same order. We give figure 3 the cartesian coordinates of the points of $\mathcal{V}_4$, and in figure 4 we represent the points of $\mathcal{V}_4$ using the projection π.

v_0	a	$(1, 0, 0)$
v_1	b	$(1, 1, 0)$
v_2	c	$(1, 1, 1)$
v_3	d	$(2, 1, 0)$
v_4	e	$(2, 1, 1)$
v_5	f	$(2, 2, 1)$

v_6	g	$(3, 1, 0)$
v_7	h	$(3, 1, 1)$
v_8	i	$(3, 2, 0)$
v_9	j	$(3, 2, 1)$
v_{10}	k	$(3, 2, 2)$
v_{11}	l	$(3, 3, 1)$
v_{12}	m	$(3, 3, 2)$

v_{13}	n	$(4, 1, 0)$
v_{14}	o	$(4, 1, 1)$
v_{15}	p	$(4, 2, 1)$
v_{16}	q	$(4, 3, 0)$
v_{17}	r	$(4, 3, 1)$
v_{18}	s	$(4, 3, 2)$
v_{19}	t	$(4, 3, 3)$
v_{20}	u	$(4, 4, 1)$
v_{21}	v	$(4, 4, 3)$

Figure 3: Visible points $\mathcal{V}_4$ (number, name, coordinates) grouped by layers of x.

In a chamfer mask, a weighting (x, y, z, w) generates by translation the *periods* $(2x, 2y, 2z, 2w)$, $(3x, 3y, 3z, 3w)$, etc. To get the homogeneity property of definition 2, it is self-evident that a mask should be only formed of visible points.

4 Farey

The *Farey series* F_n are the increasing sequences of fractions in their lowest terms, between 0 and 1, whose denominator does not exceed n [Har78]. They are the fundamental theoretical element on which are lying the properties and norm conditions of chamfer masks in 2D [Thi94]. Their extension to $\mathbb{Q}^2$ are Farey sets [Gra92].

Definition 6 (Farey set) *Farey sets* $\widehat{F}_n$ *of order* n *are sets of points* $\left(\frac{y}{x}, \frac{z}{x}\right)$ *in their lowest terms, i.e* $\gcd(x, y, z) = 1$*, between* $[0, 0]$ *and* $[1, 1]$ *whose denominator does not exceed* n*.*

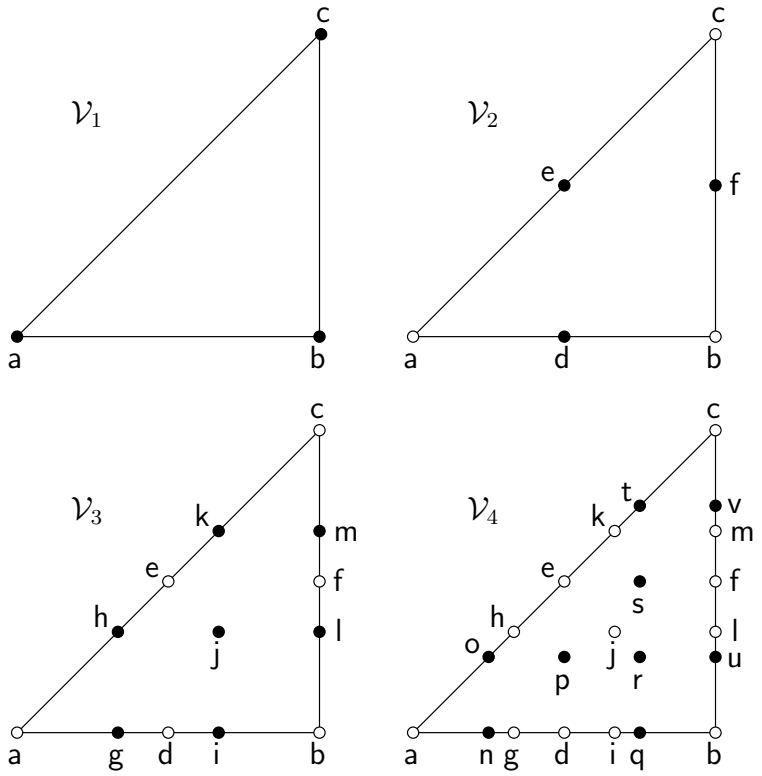

Figure 4: Visible points in projection (point • of $\mathcal{V}_n \setminus \mathcal{V}_{n-1}$, point ∘ of $\mathcal{V}_{n-1}$).

So, $\left(\frac{y}{x}, \frac{z}{x}\right) \in \widehat{F}_n$ if $x \le n$, $0 \le y \le x$, $0 \le z \le x$, and if $\gcd(x, y, z) = 1$. Therefore $(x, y, z) \in \mathcal{V}_n$ or $(x, z, y) \in \mathcal{V}_n$ by (11), and from (3) it comes the correspondence between visible points in $\mathbb{Q}^2$ and $\mathbb{Z}^3$

$$\widehat{F}_n = \left\{ \left(\frac{y}{x}, \frac{z}{x}\right) : (x, y, z) \in \mathcal{V}_n \cup \sigma_1(\mathcal{V}_n) \right\} . \tag{12}$$

The application mapping (x, y, z) to $\left(\frac{y}{x}, \frac{z}{x}\right)$ is the projection π, defined in §2 with (2). For all point A of $\mathbb{Z}^3$ we denote $\widehat{A} = \pi(A)$ the corresponding point in $\mathbb{Q}^2$. We define $\widehat{+}$ in $\mathbb{Q}^2$ by

$$\left(\frac{y}{x}, \frac{z}{x}\right) \widehat{+} \left(\frac{y'}{x'}, \frac{z'}{x'}\right) = \left(\frac{y + y'}{x + x'}, \frac{z + z'}{x + x'}\right) . \tag{13}$$

Given two points $\widehat{A}$ and $\widehat{B}$ of $\mathbb{Q}^2$, we call *mediant* of $\widehat{A}$ and $\widehat{B}$ the point $\widehat{A}\widehat{+}\widehat{B}$. From (13) we see that $\widehat{A}\widehat{+}\widehat{B}$ corresponds to $A + B$ in $\mathbb{Z}^3$, that is to say

$$\pi(A)\widehat{+}\pi(B) = \pi(A + B) . \tag{14}$$

Let (Q, R, S) be a triple of points of $\mathbb{Z}^3$. We denote $\Delta_{Q,R,S}$ the integer

$$\Delta_{Q,R,S} = \begin{vmatrix} x_Q & x_R & x_S \\ y_Q & y_R & y_S \\ z_Q & z_R & z_S \end{vmatrix} \tag{15}$$

which is the signed volume of the parallelepiped (O, Q, R, S) (cf §6.1).

Definition 7 (regular triangle) *A triple (Q, R, S) of points of $\mathbb{Z}^3$ forms a regular triangle if $\Delta_{Q,R,S} = \pm 1$.*

If $\Delta_{Q,R,S} = \pm 1$ then (OQ, OR, OS) forms a base of $\mathbb{Z}^3$, but we only focus on the subspace generated by positive linear combinations of the base vectors, as seen §5.1. Actually, a regular triangle corresponds to the notion of *consecutive* points in a Farey serie, and has the following properties.

Theorem 1 (Minkowsky) *The parallelepiped (O, Q, R, S) does not contain any point of the fundamental lattice of $\mathbb{Z}^3$ other than its vertices iff $\Delta_{Q,R,S} = \pm 1$* [Har78]. *A point is said to be* contained *in an object, if it is included in its interior, border or vertices.*

Therefore, if 3 visible points (Q, R, S) form a regular triangle, then the parallelepiped (O, Q, R, S) does not contain any other visible point (figure 5).

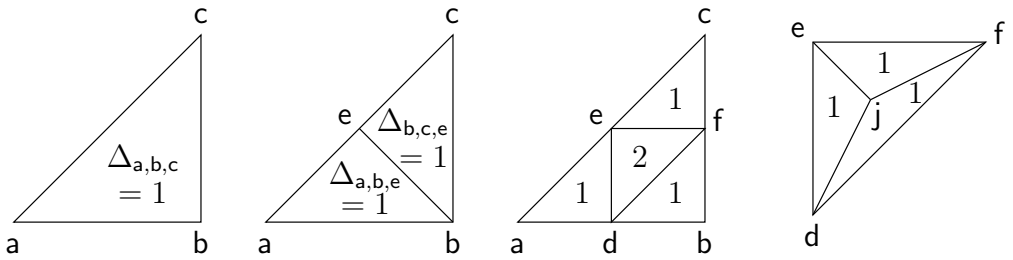

Figure 5: Regular triangles (in projection) with visible points. The triple $(\mathsf{d}, \mathsf{f}, \mathsf{e})$ is not a regular triangle since $\Delta_{\mathsf{d},\mathsf{f},\mathsf{e}} = 2$; in fact, the parallelepiped $(O, \mathsf{d}, \mathsf{f}, \mathsf{e})$ contains j.

When 3 points are consecutive in a Farey serie, the second point is the mediant of the two others [Har78]. In Farey sets this is written:

Theorem 2 (Mönkemeyer) *Let $(\widehat{Q}, \widehat{R}, \widehat{S})$ be a regular triangle of $\widehat{F}_n$. Let $\widehat{P}$ be a point of $\widehat{F}_{n+1}$, included in the triangle and distinct from the vertices; then $\widehat{P}$ is the mediant of 2 of the vertices* [Gra92].

A *Farey triangulation* denoted F_n^{Δ} , also known as *Farey net*, is the Farey set $\widehat{F}_n$, associated with a triangulation on points of $\widehat{F}_n$, such that all the triangles are regular. The triangulation in the Farey series is always unique; in a Farey set, it is almost never unique. A sequence of Farey triangulations is said to be *compatible* if the triangulation of F_n^{Δ} is a refinement of the triangulation of F_{n-1}^{Δ}.

By the theorem 2 we have a construction process of $\widehat{F}_{n+1}$ from a F_n^{Δ}. The figure 6 gives some examples of compatible triangulations.

5 Geometry of the ball

5.1 Influence Cone

We call *cone* (Q, R, S) the subspace of $\mathbb{S}$ delimited by the planes (O, Q, R), (O, R, S) and (O, S, Q). A cone (Q, R, S) is said *regular* if the triangle (Q, R, S) is regular.

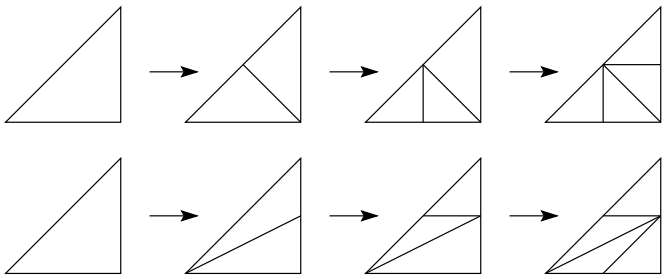

Figure 6: Compatible sequences of Farey triangulations in $\widehat{F}_2$.

Theorem 3 *If a cone (Q, R, S) is regular, then every point of the cone is reached by a path starting from O, only formed with the displacements Q, R and S [Rem00].*

Every point P of a regular cone (M_i, M_j, M_k) is therefore reached from O by a path $n_iM_i + n_jM_j + n_kM_k$. The cost of this path is $W = n_iw_i + n_jw_j + n_kw_k$ from definition (6). The distance $d_{\mathcal{M}}(O, P)$ is W if this cost is the minimum of the costs of every path reaching P. In this case, only the weightings M_i, M_j and M_k are involved in the computation of the distance.

Definition 8 (Influence cone) *We call influence cone (M_i, M_j, M_k) a regular cone in which only the weightings M_i, M_j and M_k of the mask are involved in the computation of the distance from O to any point of the cone.*

The notion of influence cone is the expression of the triangular inequality on a weighted lattice: a path of the influence cone is the "most direct" possible in the lattice associated with the mask.

5.2 Elementary displacements

In the following, we denote $\Delta_{i,j,k} = \Delta_{M_i,M_j,M_k}$. We define the discrete gradient (dx, dy, dz) using the elementary displacements :

Definition 9 (Elementary displacements) *We call elementary displacements dx, dy or dz, the cost of a unit-length displacement along x, y or z, respectively.*

Theorem 4 *In an influence cone (M_i, M_j, M_k), the elementary displacements are constant in the whole cone and their values are (see [Rem00]) :*

$$dx = \frac{1}{\Delta_{i,j,k}} \begin{vmatrix} y_i & y_j & y_k \\ z_i & z_j & z_k \\ w_i & w_j & w_k \end{vmatrix}, \; dy = \frac{-1}{\Delta_{i,j,k}} \begin{vmatrix} x_i & x_j & x_k \\ z_i & z_j & z_k \\ w_i & w_j & w_k \end{vmatrix}, \; dz = \frac{1}{\Delta_{i,j,k}} \begin{vmatrix} x_i & x_j & x_k \\ y_i & y_j & y_k \\ w_i & w_j & w_k \end{vmatrix}. \qquad (16)$$

Elementary displacements in a cone are obviously to be considered between any two 6-neighbour points both included in this cone (a cone might not always be 6-connected).

We remark that if $\Delta_{i,j,k} \neq \pm 1$, i.e (M_i, M_j, M_k) is not a regular triangle, then the elementary displacements, computed using theorem 4, may not be integers. In the distance map, displacement values are no more constant but periodical, and theses values can be found again by average among the period.

In figure 7, we give the computing formulas of the elementary displacements from theorem 4, applied to regular triangles of visible points.

Triangle	dx	dy	dz
(a, b, c)	a	b − a	c − b
(a, b, e)	a	b − a	e − a − b
(b, c, e)	e − c	b + c − e	c − b
(a, d, e)	a	d − 2a	e − d
(d, b, e)	d − b	2b − d	e − d
(b, f, e)	b + e − f	f − e	f − 2b
(f, c, e)	e − c	f − e	2c − f

Figure 7: Elementary displacements in regular triangles.

5.3 Discrete polyhedron

An important corollary of theorem 4 is that the intersection of an influence cone with its ball $B_{\mathcal{M}}(R)$ is

$$x\,dx + y\,dy + z\,dz \leq R \tag{17}$$

which is the equation of a discrete half-space, whose normal is (dx, dy, dz). If a partition of the mask's generator in influence cones exists, then the chamfer ball is a discrete polyhedron.
Such a partition corresponds to a Farey triangulation of the mask's weightings by definition. In part §6, we determine from a given Farey triangulation, the exact constraints to be satisfied on the mask's weights, so that the triangulation will correspond to the actual influence cones.

5.4 Equivalent rational ball

Given a mask $\mathcal{M} = \{\, M_i(x_i, y_i, z_i, w_i) \,\}$, we consider the integer $R = \prod_k w_k$, and we define the points $M_i'' = \frac{R}{w_i} M_i$. For every i we have

$$\frac{R}{w_i} = \frac{\prod_k w_k}{w_i} = \prod_{k \neq i} w_k \tag{18}$$

which is an integer, thus M_i'' is a period of M_i; since $d_{\mathcal{M}}(O, M_i) = w_i$ by definition, we have

$$d_{\mathcal{M}}(O, M_i'') = \prod_{k \neq i} w_k \,.\, d_{\mathcal{M}}(O, M_i) = \prod_{k \neq i} w_k \,.\, w_i = R\,. \tag{19}$$

Let us consider now the ball $B_{\mathcal{M}}(R)$ defined by (8). Every point M_i'' belongs to the ball, since by (19) its distance to O is exactly R. This means that M_i'' is a border point of the ball in the direction (O, M_i):

Theorem 5 *For every weighting M_i of the mask $\mathcal{M}$, the point M_i'' is the last point of the ball $B_{\mathcal{M}}(R)$ on the line (O, M_i).*

The ball is a discrete polyhedron based on the influence cones, therefore the points M_i'' are the vertices of the polyhedron. The coordinates of the points M_i'' are $\left(\frac{R}{w_i}x_i, \frac{R}{w_i}y_i, \frac{R}{w_i}z_i\right)$. The geometry of the ball remains the same while changing the arithmetical radius R. It is therefore interesting to take this radius back to 1 to simplify computations.

Definition 10 (Equivalent rational ball) *We call equivalent rational ball $B'_{\mathcal{M}}$ the ball with vertices $M'_i\left(\frac{x_i}{w_i}, \frac{y_i}{w_i}, \frac{z_i}{w_i}\right)$ in $\mathbb{Q}^3$.*

6 Norm conditions

We want to establish the exact conditions for a chamfer mask to induce a norm. Our strategy is based of theorem 6, which gives the norm condition under a geometrical aspect.

Theorem 6 *A function is a norm iff its ball is convex, symmetric and homogeneous* [Ber78].

By construction, every chamfer mask is symmetric towards the origin, so the chamfer ball is symmetric. In the previous section, we showed that the chamfer ball is a discrete polyhedron. We will now make this polyhedron convex and homogeneous, from a local convexity criterion between two faces of the polyhedron, and then from the gathering of these local convexities inside a Farey triangulation.

6.1 Signed volumes

Let P, Q, R, S be points of $\mathbb{Z}^3$; we denote $\delta^p(P, Q, R, S)$ the signed volume of the oriented parallelepiped, defined by the vectors $\overrightarrow{PQ}$, $\overrightarrow{PR}$ and $\overrightarrow{PS}$,

$$\delta^p(P,Q,R,S) = \begin{vmatrix} x_Q & x_R & x_S & x_P \\ y_Q & y_R & y_S & y_P \\ z_Q & z_R & z_S & z_P \\ 1 & 1 & 1 & 1 \end{vmatrix}; \tag{20}$$

The trihedron $(\overrightarrow{PQ}, \overrightarrow{PR}, \overrightarrow{PS})$ is right-handed if $\delta^p(P, Q, R, S) > 0$, left-handed if $\delta^p < 0$; the points P, Q, R, S are coplanar iff $\delta^p = 0$.

6.2 Local convexity criterion

We will establish the local convexity criterion between 2 faces of the chamfer ball in term of constraints on the weights w_i. The key point of the reasoning is to go back to the equivalent rational ball $B'_{\mathcal{M}}$ (cf §5.4).

The weightings of a chamfer mask $\mathcal{M}$ being $M_i(x_i, y_i, z_i, w_i)$, the vertices of $B'_{\mathcal{M}}$ are $M'_i\left(\frac{x_i}{w_i}, \frac{y_i}{w_i}, \frac{z_i}{w_i}\right)$. We denote $\delta'_{i,j,k,l} = \delta^p(M'_i, M'_j, M'_k, M'_l)$ and $\Delta_{i,j,k} = \delta^p(O, M_i, M_j, M_k)$.

We choose 4 weightings M_p, M_q, M_r and M_s of $\mathcal{M}$, defining 2 oriented regular triangles (M_p, M_q, M_s) and (M_q, M_r, M_s). Two triangles are said to be locally convex on $B'_{\mathcal{M}}$ if $\delta'_{p,q,r,s} \geq 0$. Factoring the $\frac{1}{w_i}$, we have

$$\delta'_{p,q,r,s} = \frac{1}{w_p w_q w_r w_s} \begin{vmatrix} x_q & x_r & x_s & x_p \\ y_q & y_r & y_s & y_p \\ z_q & z_r & z_s & z_p \\ w_q & w_r & w_s & w_p \end{vmatrix}, \tag{21}$$

whose expansion with respect to last line gives

$$\delta'_{p,q,r,s} = \frac{1}{w_p w_q w_r w_s} \left(w_p \Delta_{q,r,s} - w_q \Delta_{r,s,p} + w_r \Delta_{q,s,p} - w_s \Delta_{q,r,p} \right) . \tag{22}$$

The local convexity condition $\delta'_{p,q,r,s} \geq 0$ is then written by (22):

Theorem 7 (Local convexity criterion) *Let (M_p, M_q, M_s) and (M_q, M_r, M_s) be 2 oriented regular triangles. The local convexity criterion between the 2 corresponding faces on the ball, denoted* $\mathrm{LCC}(M_p, M_q, M_r, M_s)$*, is*

$$w_p \Delta_{q,r,s} - w_q \Delta_{r,s,p} + w_r \Delta_{q,s,p} - w_s \Delta_{q,r,p} \geq 0 . \tag{23}$$

6.3 Global convexity and homogeneity

Consider a 48-symmetric chamfer mask $\mathcal{M}$, whose generator is formed of visible points, and a Farey triangulation of these points.

The global convexity is obtained with a LCC system between all couples of adjacent triangles where at least one of them is interior to $\mathbb{S}$. If in the couple, one of the triangle is exterior, then it is symmetric to the interior triangle.

The theorem 7 translates the LCCs in a system of constraints on the weights. If the mask's weightings satisfy this system, then the facetization of the ball is convex. Moreover, the facetization of the ball (i.e the splitting into influence cones) corresponds by construction to the Farey triangulation of the beginning, and so every triangle of the triangulation defines its own influence cone.

We deduce by §5.3 that the chamfer ball is a convex discrete polyhedron made of influence cones. Since the influence cones are homogeneous, the theorem 6 is satisfied and the mask actually induces a norm.

The choice of a Farey triangulation guarantees that every corresponding cone is regular. If a LCCs system is established for a triangulation which is not Farey, then the elementary displacements may not be constant in some cones (homogeneity is lost), in particular when the determinants are not divisible by $\Delta_{i,j,k}$ in (16). In this case, the corresponding face is not delimited by a discrete plane, but is for instance jagged, or presents a light concavity.
To conclude, the construction of the generator of a chamfer mask is done in four steps:

1. take a set of visible points in $\mathbb{S}$;
2. choose a Farey triangulation of these points;
3. determine the LCCs system;
4. compute weights satisfying the LCCs.

7 Constraints

In this section, we apply theorem 7 to some small masks, so as to obtain norm constraints. In §8, we will optimize the weightings with respect to these constraints. Given a visible point v, we denote $v^i = \sigma_i(v)$; for instance b^2 stands for $\sigma_2(\mathsf{b})$.

7.1 Constraints for the mask $(\mathsf{a},\mathsf{b},\mathsf{c})$

The Farey triangulation of the mask $(\mathsf{a},\mathsf{b},\mathsf{c})$ is unique in $\mathbb{S}$. To make the ball convex and homogeneous, it is sufficient to satisfy the local convexity criteria (LCCs) from §6.2 between the face $(\mathsf{a},\mathsf{b},\mathsf{c})$ and the 3 other adjacent faces, as in figure 8-T1.

When a triangle (q,r,s) is on the border of $\mathbb{S}$, it is adjacent to its symmetric (q,s,r^i) towards the border. We note that if the edge (q,s) is changed to the edge (r,r^i), another triangulation is obtained, named co-triangulation, which is "astride" $\mathbb{S}$. Sometimes the co-triangulation is still a Farey triangulation; but adjacent faces are not the same for the LCC. This phenomenon is illustrated figure 8 with the T2 triangulation.

We extract from figure 8 the quads on which to apply the LCC; the order of the points is significant, the sign depends on it. Then we apply theorem 7 to compute the constraints on weights, and this gives the table of figure 8.

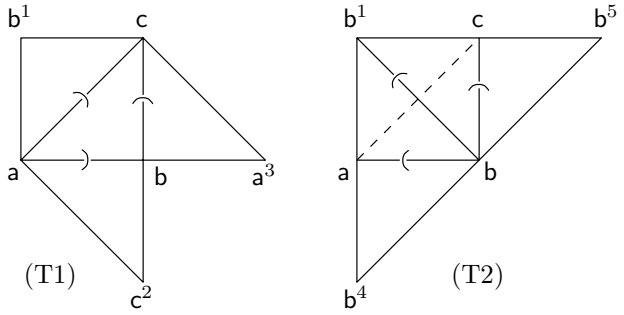

T1	$(\mathsf{a}^3,\mathsf{a},\mathsf{b},\mathsf{c})$ $(\mathsf{b}^1,\mathsf{a},\mathsf{b},\mathsf{c})$ $(\mathsf{c}^2,\mathsf{a},\mathsf{b},\mathsf{c})$	$\mathsf{b}\le 2\mathsf{a}$ $\mathsf{a}+\mathsf{c}\le 2\mathsf{b}$ $\mathsf{b}\le\mathsf{c}$
T2	$(\mathsf{b}^4,\mathsf{a},\mathsf{b},\mathsf{b}^1)$ $(\mathsf{a},\mathsf{b},\mathsf{c},\mathsf{b}^1)$ $(\mathsf{b}^5,\mathsf{b},\mathsf{c},\mathsf{b}^1)$	$\mathsf{a}\le\mathsf{b}$ $2\mathsf{b}\le\mathsf{a}+\mathsf{c}$ $2\mathsf{c}\le 3\mathsf{b}$

Figure 8: The 2 triangulations and the norm constraints for the mask $(\mathsf{a},\mathsf{b},\mathsf{c})$.

7.2 Constraints for the mask $(\mathsf{a},\mathsf{b},\mathsf{c},\mathsf{j})$

The mask $(\mathsf{a},\mathsf{b},\mathsf{c},\mathsf{j})$ is very attractive: indeed, the Farey triangulation of the mask is unique in $\mathbb{S}$ (figure 9-T1), but each of its three triangles is on a border; we have therefore the choice between edges (a,b) or $(\mathsf{j},\mathsf{j}^2)$, (b,c) or $(\mathsf{j},\mathsf{j}^3)$, (c,a) or $(\mathsf{j},\mathsf{j}^1)$: there is a total of 8 different triangulations (figure 9-T8).

Nevertheless, we observe that none of the triangles $(\mathsf{a},\mathsf{j}^2,\mathsf{j})$, $(\mathsf{j}^2,\mathsf{b},\mathsf{j})$, $(\mathsf{b},\mathsf{j}^3,\mathsf{j})$, $(\mathsf{j}^3,\mathsf{c},\mathsf{j})$, $(\mathsf{c},\mathsf{j}^1,\mathsf{j})$, $(\mathsf{j}^1,\mathsf{a},\mathsf{j})$ is a Farey triangle; so no one co-triangulation is Farey, and the T1 triangulation is the unique Farey triangulation of the mask.

The theorem 7 is applied for the T1 triangulation as depicted figure 9. One remarks that the LCC on edges (a,j), (b,j) and (c,j) is expressed by the sole LCC$(\mathsf{c},\mathsf{a},\mathsf{b},\mathsf{j})$. Finally, one sees that if the 4 weights are substitued by their Euclidean distance, the T8 triangulation is obtained, and the T1 constraints are no more satisfied.

7.3 Constraints for the mask $(\mathsf{a},\mathsf{b},\mathsf{c},\mathsf{e})$

While looking for a better approximation of d_E (see §8.4), it becomes evident that refining the mask $(\mathsf{a},\mathsf{b},\mathsf{c})$ using e is far more interesting than using j.

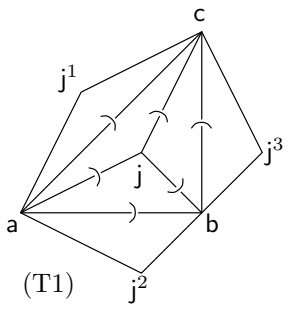

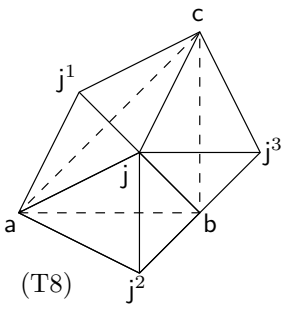

T1	(j^2, a, b, j)	$a + 2b \leq j$
	(j^3, c, j, b)	$3b + 2c \leq 2j$
	(j^1, a, j, c)	$3a + 3c \leq 2j$
	(c, a, b, j)	$j \leq a + b + c$

Figure 9: Triangulations and norm constraints for the mask (a, b, c, j).

The triangulation T1 of the mask (a, b, c, e) is unique in $\mathbb{S}$ (figure 10-T1). Considering the symmetries towards the borders, there is a total of 4 different triangulations (for instance figure 10-T4); but only T1 is Farey.

Applying the theorem 7 on the T1 triangulation gives the table of figure 10. One should notice that the LCCs on both edges (a, e) and (e, c) gives the same inequality.

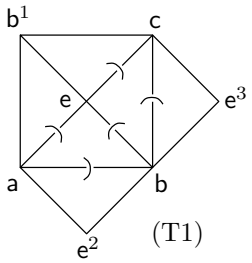

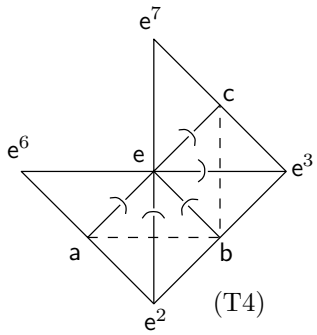

T1	(e^2, a, b, e)	$a + b \leq e$
	(e^3, b, c, e)	$b + 2c \leq 2e$
	(b^1, a, b, e)	$e \leq 2b$
	(b^1, e, b, c)	$e \leq 2b$
	(a, e, b, c)	$e \leq a + c$

Figure 10: Triangulations and norm constraints for the mask (a, b, c, e) .

8 Optimization

8.1 Relative error and scale factor

One of the chamfer mask's interest is the possibility to approximate at will the Euclidean distance d_E. First, we choose a weighting mask, which determines the computational load, but also restricts the approximation; once fixed the mask, we compute weights in order to optimize a criterion. Other needs are to be considered: for instance, it is interesting to choose small weights, to be able to keep distance maps of greater objects; so we bound to 255 the weight of a.

The error relative to d_E is computed by taking back $d_{\mathcal{M}}$ to a scale factor ε; this error is therefore $\frac{1}{\varepsilon} d_{\mathcal{M}} - d_E$. Generally $\varepsilon = a$ is taken, because this gives a coherent definition of level intervals within a distance map; but a real value may also be choosed to get closer to d_E. The error must be normalized by d_E to preserve the isotropy of the measure. Finally, the relative error is

$$G = \frac{\frac{1}{\varepsilon} d_{\mathcal{M}} - d_E}{d_E}\,, \tag{24}$$

and G is optimized for every point of $\mathbb{S}$. In every point, $d_{\mathcal{M}}$ can be computed from the influence cones and their elementary displacements. But it is far simpler to generate DT^g (fast distance transform from O in $\mathbb{S}$, detailled in [Rem00]) and to compute the relative error G on a sufficient part of DT^g. Thus, the minimal τ_{min} and maximal τ_{max} relative errors are computed. The error rate is $\tau_{\mathsf{a}} = \max(|\tau_{min}|, |\tau_{max}|)$.

The real scale factor which enables to get the error back to the mean of the interval $|\tau_{max} - \tau_{min}|$ is denoted ε_{opt}. It is proved in [Thi94] that

$$\varepsilon_{opt} = \mathsf{a}\left(\frac{\tau_{min} + \tau_{max}}{2} + 1\right) \tag{25}$$

and that the corresponding error rate τ_{opt} is

$$\tau_{opt} = \frac{\mathsf{a}}{\varepsilon_{opt}}(\tau_{max} + 1) - 1\ . \tag{26}$$

The most frequent optimization criteria in publications rely on τ_{a} and τ_{opt} [Thi94]. Formulas (25) and (26) enable to get back to Verwer's results in [Ver91b].

8.2 Optimization for the mask $(\mathsf{a}, \mathsf{b}, \mathsf{c})$

Constraints computed in §7.1 on the 2 different possible triangulations are equivalent to

$$\begin{array}{lll} \text{T1}: & \mathsf{a} \le \mathsf{b} \le 2\mathsf{a}\ , & \mathsf{b} \le \mathsf{c} \le 2\mathsf{b} - \mathsf{a}\ ; \\ \text{T2}: & \mathsf{a} \le \mathsf{b} \le 2\mathsf{a}\ , & 2\mathsf{b} - \mathsf{a} \le \mathsf{c} \le \tfrac{3}{2}\mathsf{b}\ . \end{array} \tag{27}$$

Using the following algorithm, it is possible to generate *every* possible mask

$$\text{for } \mathsf{a} = 1 \ldots 255, \text{ for } \mathsf{b} = \mathsf{a} \ldots 2\mathsf{a}, \text{ for } \mathsf{c} = \mathsf{b} \ldots \tfrac{3}{2}\mathsf{b} \tag{28}$$

giving 4.218.943 different masks. The optimization consists in generating each mask, computing for each one the error rates and keeping each mask which do better than the previous ones. The results of the optimization process using respectively the τ_{a} and τ_{opt} criteria are given in figure 11 and figure 12. The triangulation is indicated in the 4^{th} column like in (27); an $=$ means that $\mathsf{c} = 2\mathsf{b} - \mathsf{a}$, i.e that faces $(\mathsf{a}, \mathsf{b}, \mathsf{c})$ and $(\mathsf{a}, \mathsf{c}, \mathsf{b}^{\mathbf{1}})$ are coplanar.

It is interesting to note that the best rates are almost always reached by values of a about 20, and that beyond, the gain is quiet small, or even null. The τ_{a} criterion tends to center the error interval $\tau_{min} \ldots \tau_{max}$ around 0, while the τ_{opt} criterion tends to get τ_{min} back to 0.

8.3 Optimization for the mask $(\mathsf{a}, \mathsf{b}, \mathsf{c}, \mathsf{j})$

Constraints computed in §7.2 on the unique Farey triangulation T1 are equivalent to

$$\begin{array}{ll} \text{T1}: & \mathsf{a} \le \mathsf{b} \le 2\mathsf{a}\ , \quad \mathsf{b} \le \mathsf{c} \le 2\mathsf{b} - \mathsf{a}\ , \\ & \max(\mathsf{a} + 2\mathsf{b}, \tfrac{3\mathsf{b}+2\mathsf{c}+1}{2}, \tfrac{3\mathsf{a}+3\mathsf{c}+1}{2}) \le \mathsf{j} \le \mathsf{a} + \mathsf{b} + \mathsf{c}\ . \end{array} \tag{29}$$

a	b	c	T	τ_{min}	τ_{max}	τ_{a}	τ_{opt}	ε_{opt}
1	1	1	=	−42.26497	0.00000	42.26497	26.79492	0.78868
1	2	2	1	0.00000	41.42136	41.42136	17.15729	1.20711
2	2	3	2	−29.28932	6.06602	29.28932	20.00000	1.76777
2	3	3	1	−13.39746	11.80340	13.39746	12.70167	1.98406
3	4	5	=	−5.71910	10.55416	10.55416	7.94457	3.07253
5	7	8	1	−7.62396	9.54451	9.54451	8.50259	5.04801
7	9	11	=	−9.27353	7.85478	9.27353	8.62534	6.95034
10	13	16	=	−8.07612	8.62780	8.62780	8.32899	10.02758
12	16	19	1	−8.58621	8.33333	8.58621	8.47048	11.98483
17	22	27	=	−8.49206	8.30560	8.49206	8.40667	16.98415
22	29	35	1	−8.14882	8.42194	8.42194	8.27408	22.03004
29	38	46	1	−8.42030	8.26934	8.42030	8.35112	28.97811
34	45	54	1	−8.30319	8.38289	8.38289	8.33972	34.01355
39	51	62	1	−8.21611	8.34656	8.34656	8.27594	39.02544
51	67	81	1	−8.30319	8.33517	8.33517	8.31785	51.00815
56	73	89	1	−8.24255	8.33413	8.33413	8.28454	56.02564
68	89	108	1	−8.30319	8.31131	8.31131	8.30691	68.00276
85	111	135	1	−8.30319	8.30560	8.30560	8.30430	85.00102

Figure 11: Optimal masks $(\mathsf{a},\mathsf{b},\mathsf{c})$ for the τ_{a} criterion in %.

Using the scanning algorithm as (28) with the bounds (29), we are able to generate every possible mask. Due to the high number of masks, we restrict a to 200. The result of the optimization process using τ_{opt} criterion is given figure 13. This table does not include the masks where $\mathsf{j} = \mathsf{a}+\mathsf{b}+\mathsf{c}$, which are actually $(\mathsf{a},\mathsf{b},\mathsf{c})$ masks.

8.4 Optimization for the mask $(\mathsf{a},\mathsf{b},\mathsf{c},\mathsf{e})$

The greatest error relatively to d_E is reached for a point on the plane $(O,\mathsf{a},\mathsf{c})$, thus it is much more interesting to refine $(\mathsf{a},\mathsf{b},\mathsf{c})$ using the mediant of a and c, which is e, rather than j. In fact, table 14 demonstrates a better τ_{opt} (around 4 % vs. 6%). The constraints computed in §7.3 for the unique Farey triangulation T1 are equivalent to

$$\text{T1}: \quad \mathsf{a}\le\mathsf{b}\le 2\mathsf{a}\ ,\quad \mathsf{b}\le\mathsf{c}\le\tfrac{3}{2}\mathsf{b}\ ,\quad \max(\mathsf{a}+\mathsf{b},\tfrac{\mathsf{b}+2\mathsf{c}+1}{2})\le\mathsf{e}\le\min(\mathsf{a}+\mathsf{c},2\mathsf{b})\ . \tag{30}$$

8.5 3D views and conclusion

We give in figure 15, the balls $B_{\mathcal{M}}(R)$ using different chamfer masks. The sphere (a) is the ball $B_{3,4,5}(54)$, which faces $(\mathsf{a},\mathsf{b},\mathsf{c})$ and $(\mathsf{a},\mathsf{c},\mathsf{b}^1)$ are coplanars. The sphere (b) is the ball $B_{19,27,33}(342)$, which is a T1 triangulation from figure 8, and performs one of the best τ_{opt} of figure 12.

The sphere (c) is the ball $B_{11,16,19,\mathsf{j}=45}(198)$; it illustrates the T1 triangulation from figure 9, and performs one of the best τ_{opt} for the mask $(\mathsf{a},\mathsf{b},\mathsf{c},\mathsf{j})$, giving $\tau_{opt} = 5.99710\,\%$. The

a	b	c	T	τ_{min}	τ_{max}	τ_{a}	τ_{opt}	ε_{opt}
1	1	1	=	−42.26497	0.00000	42.26497	26.79492	0.78868
1	2	2	1	0.00000	41.42136	41.42136	17.15729	1.20711
2	3	3	1	−13.39746	11.80340	13.39746	12.70167	1.98406
2	3	4	=	0.00000	22.47449	22.47449	10.10205	2.22474
3	4	5	=	−5.71910	10.55416	10.55416	7.94457	3.07253
4	6	7	1	0.00000	14.56439	14.56439	6.78789	4.29129
7	10	12	1	−1.02567	12.48583	12.48583	6.38962	7.40111
11	16	19	1	−0.27586	13.18091	13.18091	6.32055	11.70978
12	17	21	1	0.00000	13.34559	13.34559	6.25538	12.80074
19	27	33	1	0.00000	13.00479	13.00479	6.10540	20.23546
26	37	45	1	−0.07399	12.85394	12.85394	6.07573	27.66139
41	58	71	1	−0.01983	12.80151	12.80151	6.02559	43.62024
183	259	317	1	0.00000	12.82262	12.82262	6.02503	194.73270
198	280	343	1	−0.00510	12.81414	12.81414	6.02382	210.68094
224	317	388	1	0.00000	12.81876	12.81876	6.02332	238.35701
239	338	414	1	0.00000	12.81197	12.81197	6.02032	254.31030

Figure 12: Optimal masks $(\mathsf{a}, \mathsf{b}, \mathsf{c})$ for the τ_{opt} criterion in %.

a	b	c	j	τ_{min}	τ_{max}	τ_{a}	τ_{opt}	ε_{opt}
8	12	14	33	0.00000	13.19231	13.19231	6.18799	8.52769
11	16	19	45	−0.27586	12.44834	12.44834	5.99710	11.66949
15	22	26	62	0.00000	12.74356	12.74356	5.99011	15.95577
26	37	45	107	−0.07399	12.58660	12.58660	5.95757	27.62664
30	43	52	123	0.00000	12.64475	12.64475	5.94642	31.89671
41	58	71	168	−0.01983	12.59174	12.59174	5.93285	43.57724
56	80	97	230	0.00000	12.60586	12.60586	5.92921	59.52964
153	217	265	627	−0.00142	12.60205	12.60205	5.92824	162.63948

Figure 13: Optimal masks $(\mathsf{a}, \mathsf{b}, \mathsf{c}, \mathsf{j})$ for the τ_{opt} criterion in %.

weighting j enables a finer (and more aesthetic) triangulation of the sphere, but does not really improve the error rate in comparison with the mask $(\mathsf{a}, \mathsf{b}, \mathsf{c})$.

The sphere (d) is the ball $B_{7,10,13,\mathsf{e}=18}(189)$, giving $\tau_{opt} = 4.6396\%$. Sphere (d) illustrates our strategy to enhance the approximation while limiting computational load: choose a refinement of the mask using a Farey mediant close to the direction of the maximal error relatively to d_E. This way, after adding e to $(\mathsf{a}, \mathsf{b}, \mathsf{c})$ to get $(\mathsf{a}, \mathsf{b}, \mathsf{c}, \mathsf{e})$ mask, the next step is to add d, giving $(\mathsf{a}, \mathsf{b}, \mathsf{c}, \mathsf{d}, \mathsf{e})$ mask.

Experimentally, tables show that the computed error rates converge to Verwer's optimal theoretical rates (see [Ver91b]), but with chamfer masks actually inducing norms. We notice that convergence is so fast that it is sufficient to use small values for a.

a	b	c	e	τ_{min}	τ_{max}	τ_{a}	τ_{opt}	ε_{opt}
3	4	5	7	−5.71910	5.40926	5.71910	5.57281	2.99535
5	7	9	13	−1.00505	9.54451	9.54451	5.05878	5.21349
7	10	12	17	−1.02567	8.79676	8.79676	4.72752	7.27199
7	10	13	18	0.00000	9.73065	9.73065	4.63960	7.34057
10	14	18	25	−1.00505	8.16654	8.16654	4.42727	10.35807
12	17	21	30	0.00000	8.65337	8.65337	4.14725	12.51920
17	24	30	42	−0.17316	8.30560	8.30560	4.07373	17.69126
24	34	42	59	0.00000	8.40723	8.40723	4.03404	25.00887
41	58	71	101	−0.01983	8.36292	8.36292	4.02353	42.71033
41	58	72	101	0.00000	8.36292	8.36292	4.01363	42.71440
53	75	92	130	0.00000	8.32724	8.32724	3.99719	55.20672
58	82	101	142	−0.04956	8.26104	8.26104	3.99142	60.38133
82	116	143	201	0.00000	8.30383	8.30383	3.98640	85.40457
111	157	193	272	0.00000	8.29265	8.29265	3.98125	115.60242
140	198	243	343	0.00000	8.28610	8.28610	3.97823	145.80027
169	239	293	414	−0.00088	8.28180	8.28180	3.97669	175.99738

Figure 14: Optimal masks $(\mathsf{a}, \mathsf{b}, \mathsf{c}, \mathsf{e})$ for the τ_{opt} criterion in %.

References

[Akt96] Z. Aktouf, G. Bertrand, and L. Perroton. A 3D-hole closing algorithm. In *Lectures Notes in Computer Science*, volume 1176, pages 36–47. Springer Verlag, 1996.

[Att97] D. Attali, G. Sanniti di Baja, and E. Thiel. Skeleton simplification through non significant branch removal. *Image Processing and Communications*, 3(3-4):63–72, 1997.

[Ber78] M. Berger. *Convexes et polytopes, polyèdres réguliers, aires et volumes*, volume 3. Cedic / Fernand Nathan, $2^{\text{ème}}$ édition, 1978. §11.8.12.

[Bor84] G. Borgefors. Distance transformations in arbitrary dimensions. *Computer Vision, Graphics and Image Processing*, 27:321–345, 1984.

[Gra92] D.J. Grabiner. Farey nets and multidimensional continued fractions. *Monatshefte für Mathematik*, 114:35–60, 1992.

[Har78] G.H. Hardy and E.M. Wright. *An introduction to the theory of numbers*. Oxford University Press, fifth edition, October 1978. §3.1.

[Rem00] E. Remy and E. Thiel. Structures dans les sphères de chanfrein. In *$12^{\text{ème}}$ congrès Reconnaissance des Formes et I.A*, Paris, Fev 2000. AFCET. Accepted.

[Ros66] A. Rosenfeld and J.L. Pfaltz. Sequential operations in digital picture processing. *Journal of ACM*, 13(4):471–494, 1966.

[San94] G. Sanniti di Baja and E. Thiel. (3,4)-weighted skeleton decomposition for pattern representation and description. *Pattern Recognition*, 27:1039–1049, 1994.

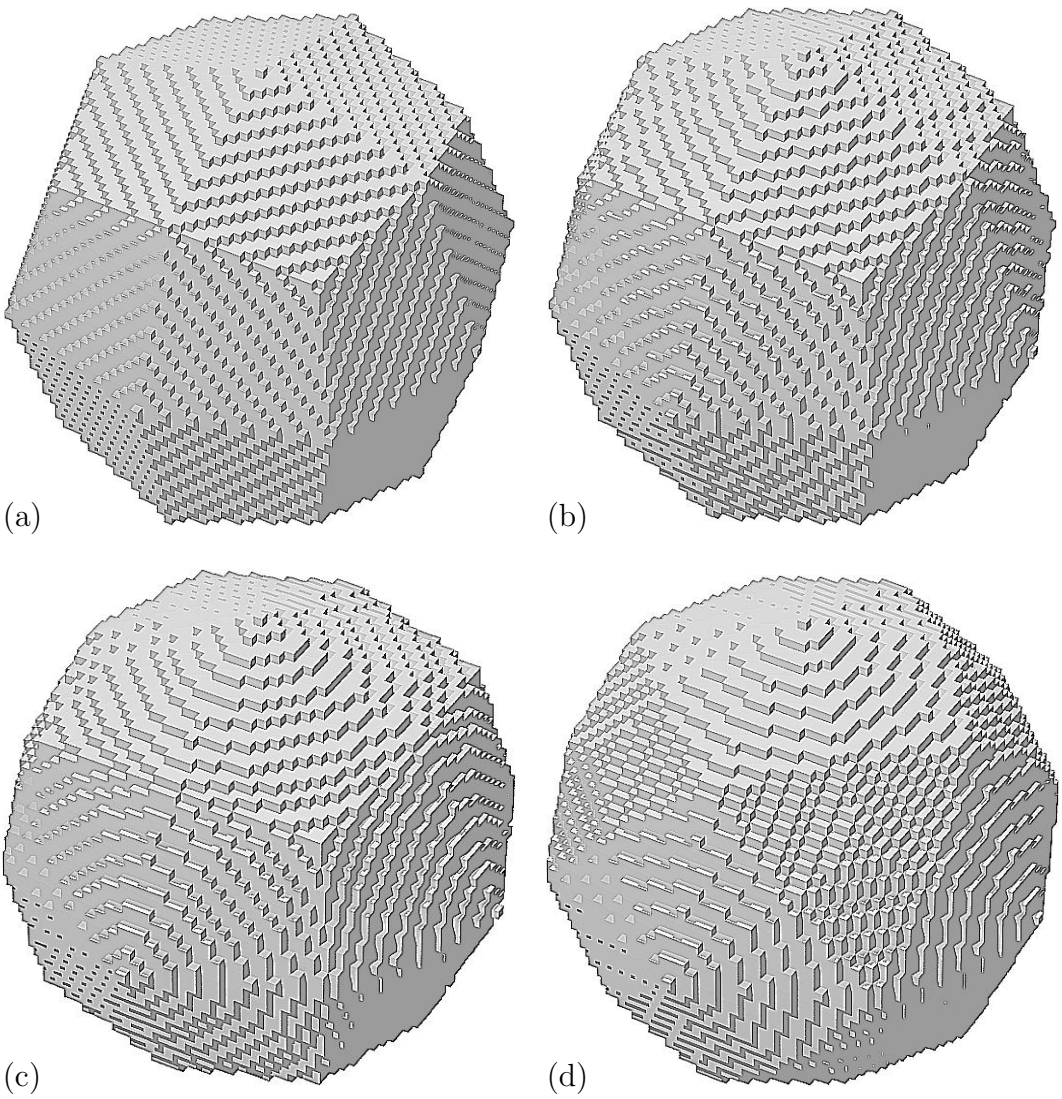

Figure 15: Chamfer spheres : (a) $B_{3,4,5}$ (b) $B_{19,27,33}$ (c) $B_{11,16,19,\mathsf{j}=45}$ (d) $B_{7,10,13,\mathsf{e}=18}$

[Thi94] E. Thiel. *Les distances de chanfrein en analyse d'images : fondements et applications*. PhD thesis, UJF, Grenoble, Sept 1994. `http://www.lim.univ-mrs.fr/~thiel/these`.

[Ver91a] J.H. Verwer. *Distance Transforms; Metrics, Algorithms and Applications*. PhD thesis, Technische Universiteit, Delft, Netherlands, june 1991.

[Ver91b] J.H. Verwer. Local distance for distance transformations in two and three dimensions. *Pattern Recognition Letters*, 12:671–682, 1991.